THEORETICAL STUDY OF IONIZATION DYNAMICS UNDER CHIRPED FEW-CYCLE LASER PULSES

H. DELIBAŠIĆ-MARKOVIĆ[1], V. PETROVIĆ[1] AND I. PETROVIĆ[2]

[1] *Faculty of Science, University of Kragujevac, Radoja Domanovića 12, 34000 Kragujevac, Serbia*
[2] *Technical Collage of Applied Studies, University of Kragujevac, Kragujevac, Serbia*

E-mail: hristina.delibasic@pmf.kg.ac.rs

Received date: 09.06.2024.

Abstract. In this paper, we investigate the ionization dynamics of Carbon, Nitrogen, Oxygen, and Phosphorus atoms subjected to chirped femtosecond laser pulses, with a focus on how chirp parameters affect ionization rates. Our analysis reveals that ionization efficiency is notably enhanced with longer pulse durations achieved through higher chirp values. This finding aligns with existing theories suggesting the pivotal role of extended laser-atom interaction times in optimizing ionization processes. Moreover, we elucidate the cumulative impact of increased pulse cycles on ionization rates, further solidifying our understanding of the ionization mechanism. This study provides valuable insights for optimizing laser parameters in applications requiring precise ionization control, advancing our understanding of ultrafast laser-atom interactions.

Key words: chirped laser pulses; tunneling ionization; ionization rate.

1. INTRODUCTION

The interaction of ultrafast laser pulses with matter, a subject at the center of modern laser physics, has generated a wealth of groundbreaking research over the past few decades [1-3]. Seminal works in this field [4-6] have elucidated the complex dynamics of atomic and molecular ionization, highlighting the pivotal role of laser parameters such as intensity, pulse duration, and, notably, chirp in dictating the ionization outcomes. Chirped femtosecond laser pulses, characterized by their time-dependent frequency modulation, have emerged as a crucial tool for manipulating ionization processes, offering a nuanced control over atomic and molecular dynamics that was previously unattainable. Research exploring the impact of chirp on ionization rates has spanned both theoretical [7, 8] and experimental [9, 10] research, with studies demonstrating how variations in chirp parameters can significantly alter the energy distribution and dynamics of ejected electrons. Experiments employing chirped laser pulses have provided valuable insights into the mechanisms of tunneling ionization and multi-photon processes, underscoring the influence of pulse shaping on the efficiency and selectivity of ionization events. These experimental findings, supported by theoretical models, have laid the groundwork for a deeper

understanding of laser-matter interaction, propelling advancements in fields ranging from attosecond physics to materials science.

In this study, we develop a comprehensive theoretical framework to analyze the ionization dynamics of Nitrogen (N), Oxygen (O), Carbon (C), and Phosphorus (P) atoms under the influence of chirped femtosecond laser pulses. Our investigation centers on how the variation in chirp parameters affects the ionization rates of these key atoms, which play crucial roles in biological molecules and materials science [11]. We offer novel insights into the modulation of ionization processes by chirp-induced pulse shaping. This approach allows for a detailed examination of the interaction between ultrafast laser pulses and atomic systems, with implications for optimizing laser applications in various scientific and technological domains. All equations and results are presented in atomic units for consistency and clarity. The structure of the paper is as follows: The Section 1 provides an overview of the theoretical and experimental background relevant to our study, positioning our work within the broader context of ultrafast laser physics and its application to ionization dynamics. Section 2 details the theoretical framework we employ to model the interaction of chirped femtosecond laser pulses with atoms. In Section 3, we present our results and engage in a discussion of the ionization dynamics of N, O, C, and P atoms as modulated by various chirp parameters, drawing connections to potential applications. Our findings underscore the pivotal role of pulse chirping in enhancing ionization efficiency and offer guidelines for tailoring laser parameters to specific ionization goals. The paper concludes with a summary of our main contributions and suggestions for future research directions in Section 4, emphasizing the significance of our theoretical insights.

2. THEORETICAL FRAMEWORK

In the field of laser physics, the study of chirped laser pulses, which exhibit a time-dependent frequency variation, is crucial in both experimental and theoretical research [12-14]. These pulses are broadly classified into linear and nonlinear types [15], each playing a significant role in probing dynamic interference phenomena, not just in individual atoms but in groups of atoms and molecules. The primary objective of this paper is to investigate the influence of various chirped pulse forms on the ionization dynamics of atoms - N, O, C, and P - that are essential in the construction of various biological molecules and materials [11]. This comprehensive analysis aims to bridge the gap between experimental and theoretical insights, emphasizing both the commonalities and distinctions in outcomes attributed to the diverse pulse types. The central focus of our investigation revolves around a chirped femtosecond laser pulse characterized by a Gaussian profile, similar to those referenced in several prominent studies [12, 15-17]. This laser pulse is linearly polarized along the z −axis and is described by the following vector potential equation:

$$\boldsymbol{A}(N,\xi,I,t) = A_0(\xi,I)f(N,\xi,t)\sin[\omega(N,\xi,t)t+\varphi_0]\boldsymbol{e}_z, \quad (1)$$

where ξ is the chirped parameter, $A_0(\xi,I)$ is the peak amplitude, $f(N,\xi,t)$ is the time-dependent envelope, $\omega(N,\xi,t)$ is the instantaneous carrier frequency, and φ_0 is the carrier-envelope phase (CEP) of the laser pulse. In the context of this research, it is presupposed that $\varphi_0 = 0$ for all computational analyses henceforth presented in this document. The peak amplitude $A_0(\xi,I)$ in Eq. (1), is defined as [12]:

$$A_0(\xi,I) = \frac{E}{\omega_0} = \sqrt{\frac{I}{I_{\mathrm{au}}\sqrt{1+\xi^2}}}. \quad (2)$$

Here, E is the amplitude of the electric field, ω_0 is the central frequency, while I and I_{au} denotes peak intensity and the laser intensity of 1 atomic unit (a.u.) (note that $1\ \mathrm{a.u.} = 3.51\times10^{16}\ \mathrm{W/cm^2}$), respectively. Building upon Eq. (1), our theoretical framework incorporates the mathematical expression of the time-dependent envelope, denoted as $f(N,\xi,t)$, which is pivotal to our analysis. This function is defined as follows:

$$f(N,\xi,t) = \exp\left[-4\ln(2)\frac{1}{1+\xi^2}\left(\frac{t}{\tau_0(N)}\right)^2\right], \quad (3)$$

where $\tau_0(N)$ represents the pulse duration. This parameter is inherently related to the pulse's temporal structure and can be further expressed in terms of the number of cycles, N, and the central angular frequency of the pulse, ω_0, specifically: $\tau_0(N) = 2N\pi/\omega_0$. Finally, in the context of our theoretical framework, it is crucial to incorporate the parameter $\omega(N,\xi,t)$, representing the instantaneous carrier frequency, following the detailed description of the vector potential in Eq. (1). This parameter is fundamental to the temporal analysis of the chirped laser pulse, as it describes the variation in the pulse's frequency at any given moment. The instantaneous carrier frequency is defined mathematically as:

$$\omega(N,\xi,t) = \omega_0 + 4\ln(2)\frac{\xi}{1+\xi^2}\frac{t}{\tau_0(N)^2}. \quad (4)$$

The thorough examination of the vector potential $\boldsymbol{A}(N,\xi,I,t)$ and its components (see Eqs. (2)-(4)) sets the stage for elucidating the electric field strength $\boldsymbol{E}(N,\xi,I,t)$ of the laser pulse, which is crucial for the study of ionization dynamics. The strength of the electric field can be analytically derived from the temporal derivative of the vector potential, $\boldsymbol{E}(N,\xi,I,t) = -\partial\boldsymbol{A}(N,\xi,I,t)/\partial t$, establishing a direct correlation between the temporal evolution of the vector potential and the resulting electric field encountered by atomic particles. For our analysis, particularly within the scope of tunneling ionization, we present the following analytical representation of the electric field:

$$\boldsymbol{E}(N,\xi,I,t) = 2^{1-\Xi(N,\xi)t^2}\, t\, A_0(\xi,I)\ln(2)\times$$
$$\times\{\xi\cos[\xi t^2\,\Xi(N,\xi)\ln(2)+\omega_0]-\sin[\xi t^2\,\Xi(N,\xi)\ln(2)+\omega_0]\}\,\boldsymbol{e}_z, \qquad (5)$$

where $\Xi(N,\xi) = {\omega_0}^2/\{\pi^2N^2(1+\xi^2)\}$ is introduced to facilitate a more succinct formulation. Eq. (5) delineates the complex dependency of the electric field on the vector potential, capturing its dynamic nature in the context of the laser-matter interaction processes under study. This equation is not just a theoretical construct but a quantifiable descriptor of the laser field's influence on the ionization phenomena being investigated.

With the theoretical framework in place, we proceed to Fig. 1, which offers a graphical representation of chirped laser pulses, based on Eq. (5). These visualizations elucidate the effect of the chirp parameter on the electric field strength over time, as well as the corresponding vector potential and instantaneous frequency for non-chirped ($\xi = 0$, dotted line), positive-chirped ($\xi = 1.75$, dashed line), and negative-chirped ($\xi = -1.75$, solid line) pulses, each operating with a central frequency of $\omega_0 = 53.605$ eV. The subfigures (Fig. 1(a), Fig. 1(b), and Fig. 1(c)) display these variations across an increasing number of cycles $N = 1$, $N = 3$, and $N = 5$, respectively, demonstrating the influence of chirp on the pulse's temporal and spectral characteristics, and setting the stage for an in-depth discussion on their ionization dynamics.

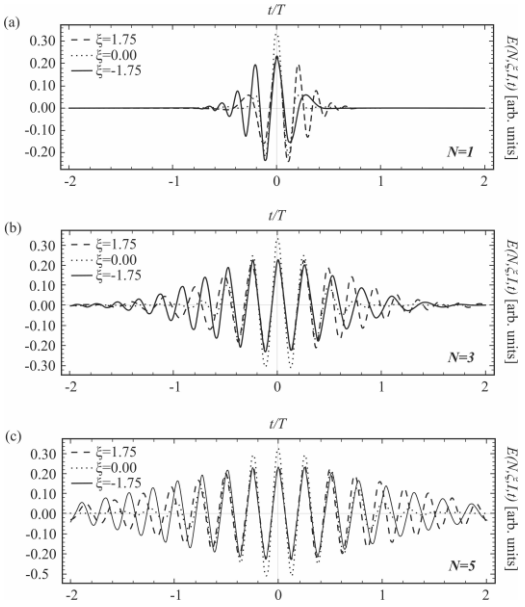

Fig. 1. The figure presents the dependency of the electric field, $E(N,\xi,I,t)$ as a function of normalized time for different chirp parameters ξ. Each panel corresponds to a different number of cycles: (a) $N = 1$, (b) $N = 3$, and (c) $N = 5$, respectively, highlighting the effects of chirp on the pulse's temporal characteristics.

From Fig. 1(a) it is possible to conclude that the non-chirped pulse ($\xi = 0$, dotted line) displays a Gaussian-like temporal profile, which is expected for a transform-limited pulse. The absence of chirp results in a balanced distribution of frequencies throughout the pulse duration. On the other hand, the positively chirped pulse ($\xi = 1.75$, dashed line) shows temporal broadening, a characteristic that has been associated with a gradual redshift in frequency components over time, in line with studies that correlate positive chirp with increased pulse durations [17]. Similarly, the negatively chirped pulse ($\xi = -1.75$, solid line) exhibits a compression in its temporal profile, indicating a blueshift, which has been shown to enhance ionization potential due to the increased field strength [12, 16]. Additionally, Fig. 1(b) with N=3 cycles, and Fig. 1(c), with $N = 5$ cycles, illustrate the scaling effect of the number of cycles on the chirped pulses. The temporal stretching for $\xi = 1.75$ and the compression for $\xi = -1.75$ become more pronounced with an increased number of cycles. This trend is consistent with the theoretical models that predict a non-linear scaling of chirp effects with the number of cycles [15]. The observed decrease in peak intensity for the positively chirped pulse and the increase for the negatively chirped pulse align with the quantum mechanical models of ionization [18], which suggest that the probability of tunneling ionization is highly sensitive to the electric field strength.

The interplay between chirp parameters and the electric field characteristics of laser pulses is a subject of extensive study due to its profound implications in the field of ultrafast optics and its applications in ionization processes. As we delve into the subtleties of how the temporal and spectral properties of laser pulses are influenced by chirping, Fig. 2 offers valuable insights. In Fig. 2, we examine the modulation of the electric field $E(N, \xi, I, t)$ by varying the number of optical cycles N and chirp parameters ξ. This analysis is critical for understanding the control mechanisms available in ultrafast laser experiments, particularly those involving the ionization of matter. As one can conclude based on the results presented in Fig. 2, panels (a), (c), and (d) showcase the alterations in the temporal profiles of chirped laser pulses, reflecting how chirping can stretch or compress the electric field over time. A positive chirp ($\xi = 1.75$) induces an extension of the pulse's temporal duration, as demonstrated by the stretched electric field signal, a phenomenon consistent with [19], who examined the relationship between chirp, pulse expansion, and subsequent ionization rates. Furthermore, negative chirp ($\xi = -1.75$) manifests as a contraction in the pulse's temporal shape, intensifying the electric field strength within a more abbreviated timeframe. This compaction of the electric field signal aligns with the observations of [20], who linked increased ionization potential with the rise in electric field strength afforded by negative chirping. Additionally, the contour plot in Fig. 2(b) provides a comprehensive view, detailing how the electric field amplitude responds to the interplay between chirp parameter variations and the number of optical cycles, a relationship intricately explored by [21]. This graphical

representation serves as a comprehensive overview, illustrating the complex ways in which chirping can be leveraged to manipulate pulse characteristics for tailored interaction with atoms and molecules.

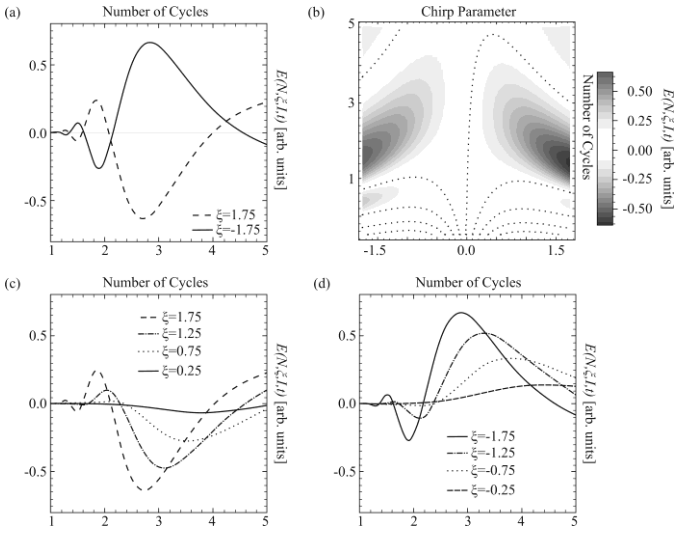

Fig. 2. The figure presents the dependency of the electric field, $E(N, \xi, I, t)$, on the number of optical cycles N, for varying chirp parameters ξ. Panels (a), (c), and (d) detail the modulation of $E(N, \xi, I, t)$ for chirped laser pulses, where the temporal profile is systematically altered by the chirp. For positive chirp values, $\xi = [0.25, 0.75, 1.25, 1.75]$, the field is temporally stretched, displaying an increase in the cycle duration, while negative chirp values, $\xi = [-0.25, -0.75, -1.25, -1.75]$ compress the cycle duration, reflecting a decrease. Panel (b) provides a contour plot which delineates the amplitude variation of $E(N, \xi, I, t)$ across both the chirp parameter space and the number of cycles.

Building upon the foundational understanding of chirped laser pulses and their role in modulating ionization dynamics, we now shift our focus to the specific mechanisms of tunneling ionization under the influence of chirped pulse excitation.

2.1. INSIGHTS INTO TUNNELING IONIZATION DYNAMICS UNDER CHIRPED PULSE EXCITATION

The ionization rate of atoms and molecules when subjected to intense laser fields is a parameter of paramount importance, shaping the frontiers of ultrafast optics and photonics. Theoretical explorations, buttressed by seminal works such as those by [22, 23], have elucidated the critical role of the electric field in steering the ionization pathway of electrons. The advent of chirped laser pulses has introduced an additional layer of control over the ionization process, as the temporal modification of the pulse can lead to a significant variance in ionization rates. This variability is rooted in the delicate interplay between the electric field's peak

intensity, its temporal spread, and the inherent phase relationship of the frequency components - factors that are deftly orchestrated through chirping. Positive chirping extends the duration of a pulse while lowering its peak intensity, which can consequently reduce ionization rates, as demonstrated in the studies referenced in [24]. Conversely, negative chirping compresses the pulse duration and enhances the peak intensity, thereby potentially increasing ionization rates, according to the findings described in [24].

As we delve into the specifics of tunneling ionization, it is imperative to consider the Landau-Dykhne adiabatic approximation, a theoretical framework for analyzing the probability amplitudes of quantum transitions in the presence of slowly varying external fields. This approach is particularly apt for chirped pulse scenarios, where the temporal evolution of the pulse can be tailored to ensure adiabaticity or to induce non-adiabatic transitions at will. The subsequent analysis in this section aims to dissect the impact of chirping on tunneling ionization rates. By integrating the insights gained from past research with the mathematical rigor of our theoretical models, we seek to advance the understanding of how chirped laser pulses can be harnessed to control and optimize ionization - a quest that remains at the center of ultrafast laser science and its myriad applications, from attosecond physics to controlled chemical reactions.

In the Landau-Dykhne adiabatic approximation, the central physical concept rests on the assumption that a quantum system can be perturbed so gently that it remains in an eigenstate of its Hamiltonian, despite the fact that the eigenvalues (and hence the eigenstates) are changing with time. The approximation is most valid when these changes occur over timescales much longer than the system's intrinsic dynamical timescale, allowing the system to adapt its state instantaneously to the slowly changing conditions. The transition amplitude $\mathcal{A}_{if}(t)$, which describes the probability amplitude for a system to evolve from an initial state 'i' to a final state 'f', is then given by the exponential of an action integral [25]:

$$\mathcal{A}_{if}(t) = \exp\left[i \int_0^\tau \left(\mathcal{E}_f(t) - \mathcal{E}_i(t)\right) dt\right], \tag{6}$$

where $\mathcal{E}_i(t)$ and $\mathcal{E}_f(t)$ are the adiabatic energy states, functions explicitly dependent on time. According to the adiabatic theorem, the system's quantum states will adiabatically follow the Hamiltonian's progression, remaining in their instantaneous eigenstates, provided that the rate of external perturbation is sufficiently gradual. The action integral, $\mathcal{S}(t)$, defined as the temporal integral of the eigenenergy differential, represents the accumulated quantum action - or the area within phase space - that the system encompasses as it transitions. This integral in Eq. (6), denoted as $\mathcal{S}(t) = \int_0^\tau \left(\mathcal{E}_f(t) - \mathcal{E}_i(t)\right) dt$, embodies the phase evolution of the system and is instrumental in characterizing the dynamics of adiabatic quantum transitions.

Delving into the behavior of quantum systems subjected to adiabatic processes, the determination of the turning point τ becomes crucial. This marks the peak susceptibility of the system to non-adiabatic transitions, effectively highlighting the potential divergence in the quantum state's trajectory under the influence of external forces. Within the framework of the Landau-Dykhne adiabatic approximation, this turning point is precisely established using the stationary-phase method, encapsulated by the expression:

$$\frac{\partial \mathcal{S}(t)}{\partial t}\Big|_{\tau} = 0. \tag{7}$$

The condition of the derivative equating to zero implies that the system's phase-space trajectory experiences a local extremum at this point. Physically, such extremization signals conditions conducive to constructive interference in the transition amplitude's phase, thereby enhancing the probability of a quantum transition. The concept of the turning point seamlessly integrates into the semiclassical interpretation of quantum mechanics, offering a nuanced understanding of how quantum states evolve under classical trajectories yet demonstrate wave-like interference patterns. At the turning point, within the complex time plane, the system finds itself at a saddle point—a decisive moment where the paths integral to the transition amplitude converges, significantly influencing the outcome of quantum transitions. When applied to the dynamics induced by chirped laser pulses, the turning point concept becomes instrumental in dissecting how adiabatic changes to the Hamiltonian precisely modulate quantum transitions. Such understanding is invaluable for tunneling ionization, where the timing and conditions dictated by the chirp can critically affect the ionization rates and influence the system's evolution post-ionization.

Following the identification of the turning point τ within the adiabatic framework, our focus shifts towards quantifying the transition dynamics between quantum states. The transition rate, $\mathcal{W}_{if}$, emerges as a key metric, encapsulating the probability of a system transitioning from an initial state 'i' to a final state 'f'. This rate can be expressed in terms of the squared modulus of the transition amplitude $\mathcal{A}_{if}(t)$, which, in physical terms, represents the probability density of such a transition occurring:

$$W_{if} = \left|\mathcal{A}_{if}(t)\right|^2 \propto \exp[-2\ \mathrm{Im}\{\mathcal{S}(t)\}]. \tag{8}$$

This representation of the transition rate emphasizes the nontrivial role of the imaginary part of the action integral, $\mathcal{S}(t)$. It illustrates how the quantum tunneling amplitude is influenced by the underlying complex phase structure of the transition amplitude. Exponential dependence is a manifestation of the semiclassical nature of the transition; it exhibits a classical action’s exponential suppression in a tunneling scenario.

Adjusting the focus from the broader theoretical frameworks to the specific phenomena at hand, our discourse shifts toward analyzing the behavior of ionization rates under the influence of chirped laser pulses. Central to this examination is the concept of the turning point, τ, which serves as a fundamental point where the conditions for quantum tunneling are met within the semiclassical approximation. This turning point is identified when the energy of an electron in its bound state, $\mathcal{E}_i(t) = -I_p$, (where I_p signifies the ionization potential), equates to its energy in the final state influenced by an external electric field, described as $\mathcal{E}_f(N,\xi,I,t) = (p + A(N,\xi,I,t)/c)^2/2$. Here, p indicates the momentum of the ejected photoelectron, and $A(N,\xi,I,t)$ denotes the electric field's vector potential as defined in Eq. (1). This equality signifies the precise moment when the electron's transition into the continuum becomes energetically viable due to energy alignment. To accurately determine τ, we integrate the conditions for stationary action with those for energy alignment. The derived formula for τ is as follows:

$$\tau(N,\xi,I,t,p) = 1 - \xi'\mathcal{A}_0(\xi,I)(c\tau_0(N))^2 \times \\ \times \frac{\left\{\left(2I_p - \varkappa(p)\right)\left(\xi + \xi'\omega(N,\xi,t)\tau_0(N)^2\omega(N,\xi,t)\right) + \left(\varkappa(p)(\xi\ln[4] + \xi'\omega(N,\xi,t)\tau_0(N)^2\right)\right)^{1/3}\right\}}{3\omega(N,\xi,t)^2\mathcal{A}_0(\xi)\Xi(N,\xi)}. \quad (9)$$

To enhance the mathematical expression's legibility in our analysis, we define concise variables: $\varkappa(p) = 2I_p - p\left(p + 2i\sqrt{2I_p}\right)$, encapsulating the interaction between ionization potential, I_p, and electron momentum, p, and $\xi' = 1 + \xi^2$, representing the adjusted chirp parameter. These notational simplifications are introduced to facilitate a more streamlined discussion of the turning point τ within the framework of our study.

Let's commence by evaluating the the time-dependent segment of the action, $\mathcal{S}(t)$, which is instrumental in determining the transition rate pertaining to tunnel ionization. Evaluation of thus quantity necessitates careful consideration of the dynamics and underlying interactions that come into play during tunneling. By focusing on it, we can isolate the temporal aspects of the ionization process and gain insight into how the action evolves over time. Proceeding with this approach, we substituted the expression for $\tau(N,\xi,I,t,p)$ from Eq. (9) into the epression for the action, $\mathcal{S}(t) = \int_0^{\tau}\left(\mathcal{E}_f(t) - \mathcal{E}_i(t)\right)dt$. This integration process yields a refined formula for $\mathrm{Im}\{\mathcal{S}(\tau)\}$, isolating the component that significantly influences the transition rate within the context of tunnel ionization as:

$$\mathcal{S}(\tau) = \int_0^{\tau}\left(\frac{A_0(\xi,I)}{2}\left(\frac{p}{A_0(\xi,I)} - \exp\left[-\frac{4\ln(2)}{1+\xi^2}\left(\frac{t}{\tau_0(N)}\right)^2\right]\sin\left[\omega_0 t + \frac{4\xi\ln(2)}{1+\xi^2}\left(\frac{t}{\tau_0(N)}\right)^2\right]\right)^2 + \right. \\ \left. + I_p\right)dt. \quad (10)$$

Upon solving integral given by the Eq. (10) we encountered significant computational challenges. The complexity of resolving the integral to extract the imaginary part of the action, $\mathrm{Im}\{\mathcal{S}(t)\}$, required meticulous analysis due to the intricate dynamics and interactions inherent in the tunneling process. To address these challenges and obtain an analytical expression for the ionization rate, we leveraged advanced numerical methods. The application of these numerical techniques enabled us to systematically dissect the temporal component of the ionization process, ultimately leading to a concise expression for $\mathrm{Im}\{S(t)\}$. The numerical approaches employed included a combination of adaptive quadrature methods for accurate integral evaluation [26] and Fourier transform techniques [27] to deal with the oscillatory nature of the integrand, especially due to the sinusoidal term influenced by the chirp parameter ξ and the laser's angular frequency ω_0. This comprehensive numerical analysis led to the derivation of a detailed analytical expression for the ionization rate:

$$\mathcal{W}(N,\xi,I,t,p) = \exp[-2\mathrm{Im}\{\mathcal{S}(\tau)\}] \propto$$
$$\propto \exp\Big[-2\Big((\omega(N,\xi,t)\tau_0(N)^2)^2\mathcal{A}_0(\xi,I)\Omega(N,\xi,I,p,t)\Big(1+\Omega(N,\xi,I,p)^{2/3}\Big)\times$$
$$\times\left(p^2\sqrt{2I_p}\Omega(N,\xi,I,p,t)^{1/6} - \omega(N,\xi,t)^2\mathcal{A}_0(\xi,I)^2 c{I_p}^2\tau_0(N)^2(p^2+\xi')\right], \quad (11)$$

where, to simplify the equation, we introduce the variable: $\Omega(N,\xi,I,p) = (c\tau_0)^2\xi' A_0(\xi,I)(\xi+\omega(N,\xi,t)\xi'\tau_0(N)^2)\left(2I_p - \left(p^2+2\sqrt{2I_p}\right)\right)$.This expression, derived from numerical analyses, significantly enhances our comprehension of how ionization rates can be modulated using chirped laser pulses. This breakthrough is particularly salient for atoms like N, O, C, and P, which play pivotal roles in the architecture of biological molecules and advanced materials. Gaining insight into the ionization behavior of these atoms when exposed to chirped pulses provides a powerful means to alter their electronic configurations, an essential aspect for a range of applications including material ablation, the synthesis of nanoparticles, and optimizing the laser-induced breakdown (LIB) process for precise tissue analysis with minimal side effects. Research, such as the work by [28] that delves into laser-induced damage thresholds within biological contexts, highlights the significance of mastering ionization rates for practical outcomes.

3. RESULTS AND DISCUSSION

This section examines the impact of chirped laser pulses on the ionization dynamics of N, O, C, and P atoms. Our study focuses on the effects of varying chirp parameters, $\xi = \pm 1.75$, and the number of cycles, $N = 1-5$, on the calculated ionization rate $\mathcal{W}(N,\xi,I,t,p)$, as introduced in Eq. (11). The atoms selected for this analysis are integral to a wide array of biological molecules and materials, underscoring the relevance of our findings across various scientific and technological

fields. To ensure our results are comparable with existing studies, we set the central carrier frequency of the laser pulse to $\omega_0 = 53.605$ eV, in accordance with [29]. Pulse durations were chosen as 5 fs and 50 fs to cover a broad range of interaction times, and the laser intensity was varied between 1×10^{16} W/cm^2 to 1×10^{18} W/cm^2.

First, Fig. 3 presents the ionization rate, $\mathcal{W}(N, \xi, I, t, p)$, for N, O, C, and P atoms, illustrating the dependency on laser intensities that range from 1×10^{16} W/cm^2 to 1×10^{18} W/cm^2. Each graph within the figure is fixed at a cycle number $N = 5$ and displays the ionization rates under distinct chirped laser conditions, characterized by the chirp parameters: (a) $\xi = 0.25$, (b) $\xi = 0.75$, (c) $\xi = 1.25$, and (d) $\xi = 1.75$. This constant cycle number provides a uniform basis for comparison across different chirping conditions, showcasing the influence of laser intensity and chirp on ionization. The series of plots delineate the response of each atom - N (solid line), O (dashed line), C (dotted line), and P (dot-dashed line) - to the various intensities of the laser field, under a precise chirp-induced temporal shaping of the laser pulse.

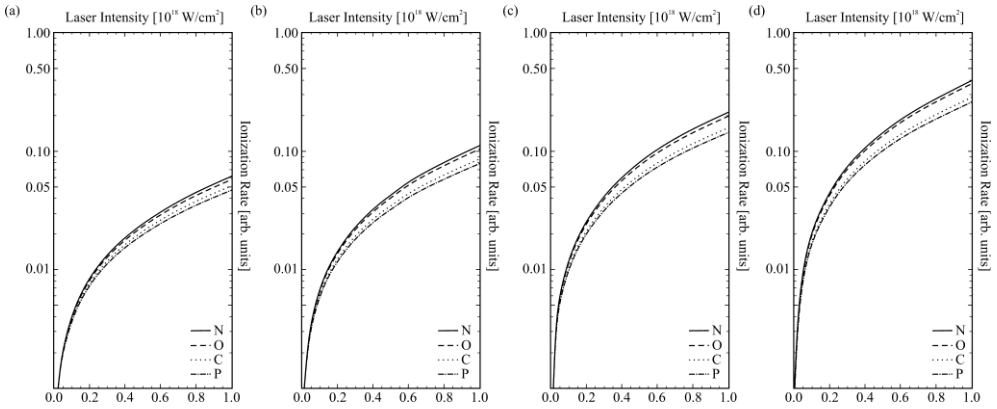

Fig. 3. Ionization rates $\mathcal{W}(N, \xi, I, t, p)$ for N, O, C, and P atoms at a constant cycle number $N = 5$, plotted against laser intensities ranging from 1×10^{16} W/cm^2 to 1×10^{18} W/cm^2, under various chirp conditions: (a) $\xi = 0.25$, (b) $\xi = 0.75$, (c) $\xi = 1.25$, and (d) $\xi = 1.75$.

Within each sub-figure from Fig. 3(a) to 3(d), representing different chirp parameters ($\xi = 0.25$ to $\xi = 1.75$), the ascending curves with laser intensity suggest a non-linear ionization process. Such behavior, which deviates from simple linear scaling with intensity, is corroborated by the findings in recent studies [30, 31], affirming that the ionization rates are significantly influenced not just by the magnitude of the laser intensity but by the temporal shaping of the pulse due to the chirp parameter. At lower chirp values, such as $\xi = 0.25$ (Fig. 3(a)), despite the theory suggesting enhanced ionization due to increased peak intensities, the shorter pulse duration may not provide ample energy delivery, particularly for atoms with higher ionization

thresholds. This has been observed and discussed in works such as those by [ref], where the relationship between pulse compression, peak intensity, and ionization efficiency was explored. Conversely, at a higher chirp value of $\xi = 1.75$ (Fig. 3(d)), the pulse is temporally extended, which reduces the peak intensity but lengthens the interaction window. This enables the atom to accrue energy gradually, enhancing the ionization probability over time, an effect that is notably pronounced for the P atom. This trend of increasing ionization rates with longer pulse durations at higher chirp values aligns with observations reported by [31], where the benefits of extended interaction times for efficient ionization were elucidated. This is reflective of a dynamic equilibrium between the atom's electronic structure and the energetics provided by the pulse, a nuanced interaction that can be tied to the temporal shaping of the pulse as influenced by the chirp parameter. These findings are consistent with the theoretical models presented in [32], which describe how electronic structure and ionization potential govern the atom's response to laser fields. In consideration of these trends, it is essential to account for the electronic structure and ionization potential of each element. Electrons in different atoms will absorb energy at different rates, a process dictated by the instantaneous field strength and the duration of exposure to the field. The fact that higher chirp parameters, and therefore longer pulse durations, result in increased ionization rates - even amidst reduced peak intensities - underscores the intricate balance between pulse duration and intensity in achieving optimal ionization, as discussed in comprehensive studies such as those by [33].

Next, in Fig. 4, we present the ionization rate, $\mathcal{W}(N, \xi, I, t, p)$, and its dependencies on chirp parameters, ξ, and cycle numbers, N, which are fundamental in assessing the efficiency of atomic ionization under varied laser pulse conditions. Specifically, Fig. 4(a) elucidates the variation of ionization rates with cycle numbers, N, ranging from 1 to 5 for the N atom at a constant laser intensity of $I = 5 \times 10^{17}\ \mathrm{W/cm^2}$ when the chirp parameter is fixed to the following values: $\xi = 0.25$ (solid plot), $\xi = 0.75$ (dotted plot), (c) $\xi = 1.25$ (dot-dashed plot), and $\xi = 1.75$ (dashed plot). This analysis is important as it allows us to examine the direct influence of pulse duration on ionization efficiency, a key factor in the optimization of laser-induced processes in both theoretical and applied contexts. Furthermore, Fig. 4(b) offers a contour plot for the N atom, illustrating the impact of chirp parameters, ξ, across a range of -1.75 to 1.75 and cycle numbers $N = 1 - 5$. The contour plot serves as a visual guide to understand the modulation of ionization rates by the chirp parameter, enabling us to discern how alterations in the temporal structure of the pulse translate to quantitative changes in ionization probability.

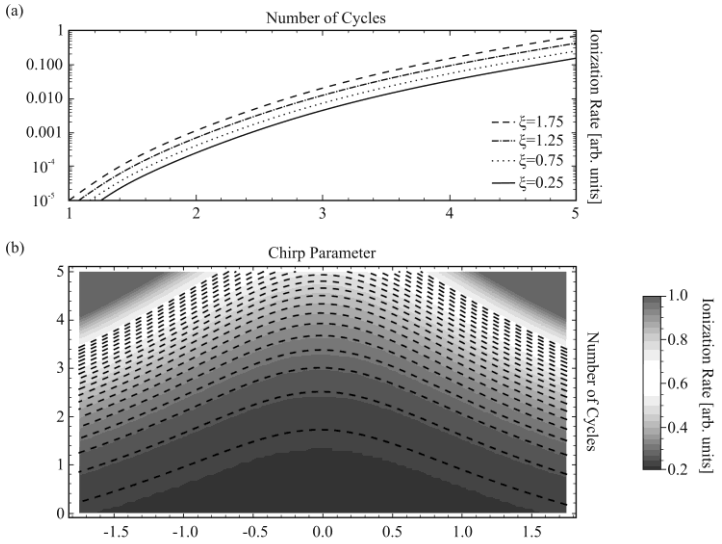

Fig. 4. Ionization rate, $\mathcal{W}(N, \xi, I, t, p)$, for the N atom dependencies on chirp parameters, ξ, and cycle numbers, N, showcasing: (a) the rate's variation with cycle numbers $N = 1 - 5$ when laser intensity is fixed to $I = 5 \times 10^{17}$ W/cm^2, with each curve representing different chirp parameters: $\xi = 0.25$, $\xi = 0.75$, $\xi = 1.25$, and $\xi = 1.75$, (b) a contour plot, illustrating the impact of chirp parameters across a ξ range of -1.75 to 1.75 and number of cycles $N = 1 - 5$.

The curves presented in Fig. 4(a) demonstrate that the ionization rate increases with the number of cycles, indicating that longer interaction times between the laser pulse and the atom generally led to more efficient ionization. These trends can be attributed to the cumulative effect of the electric field's interaction with the atomic electron over multiple cycles, effectively leading to increased energy absorption and a higher probability of overcoming the ionization threshold. The varying chirping parameters influence the temporal profile of the electric field within each cycle, thereby affecting the instantaneous intensity experienced by the atom and modulating the ionization rate accordingly. For the N atom, characterized by its specific ionization potential and electronic structure, the response to different chirp parameters can be quite nuanced. As shown by the dashed curve $\xi = 1.75$, a highly positive chirp parameter correlates with a slower rate of increase in ionization compared to less chirped pulses (as indicated by the solid line, $\xi = 0.25$). This suggests that the broadening of the pulse in time, which occurs with higher positive chirp, may lead to a reduction in peak intensity at any given time slice, thus reducing the ionization probability per cycle. Conversely, as we approach the solid plot, where the chirp parameter is closer to zero, indicating a less chirped pulse, we see a more rapid increase in ionization rate, which implies a more confined pulse in time and therefore a higher peak intensity during the interaction. Furthermore, in Fig. 4(b), the contour plot provides a visual representation of how the ionization rate for the N atom changes with both

the chirp parameter and the number of cycles. The color gradient represents different ionization rates, with warmer colors indicating higher rates, and the contour lines map regions of equal ionization rates. We can observe that at a fixed number of cycles, changes in the chirp parameter can lead to different ionization outcomes, with certain values of chirp leading to higher ionization rates than others. This visualization underscores the complex interdependence between chirp, cycle number, and ionization efficiency, offering insight into the optimal pulse configurations for maximizing ionization rates for the N atom.

Finally, results presented in Fig. 5 direct our attention specifically to the C atom and its response to varying intensities of a laser field. Here, we dissect the ionization rate, $\mathcal{W}(N,\xi,I,t,p)$, as a function of laser intensity within the range of 1×10^{16} W/cm^2 to 1×10^{18} W/cm^2, under the influence of chirped laser pulses at selected cycle numbers $N=1$ (solid line in Fig. 5), $N=3$ (dotted line in Fig. 5) and $N=5$ (dashed line in Fig. 5). The data are arrayed to reflect two distinct chirp conditions: Fig. 5(a) a lower chirp ($\xi=0.25$) and (b) a higher chirp ($\xi=1.75$), allowing for a granular assessment of chirp's role in modulating ionization processes.

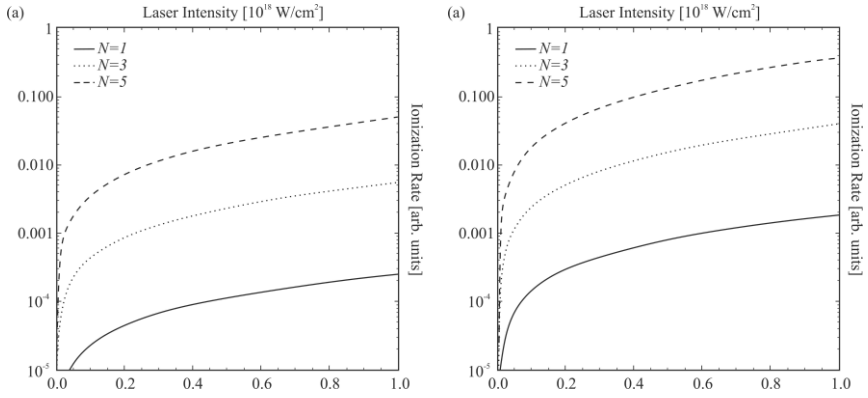

Fig. 5. Ionization rate, $\mathcal{W}(N,\xi,I,t,p)$, of a C atom as a function of laser intensity, varying $I=1\times10^{16}-1\times10^{18}$ W/cm^2, for selected cycle numbers ($N=1,3,5$). The relationship is examined under two distinct conditions: (a) $\xi=0.25$, and (b) $\xi=1.75$.

From the results presented in Fig. 5, one can conclude that the ionization rate $\mathcal{W}(N,\xi,I,t,p)$ of a C atom exhibits a dependence not only on the intensity of the laser field but also on the number of cycles of the chirped pulse. The curves for $N=1$, $N=3$, and $N=5$ signify different amounts of time that the C atom is subjected to the laser's influence within a single pulse, under two distinct chirping conditions, i.e., $\xi=0.25$ and $\xi=1.75$. For the lower chirp condition (Fig. 5(a)), the laser pulse is less stretched, implying a higher peak intensity and a shorter pulse duration. In contrast, the higher chirp (Fig. 5(b)) condition elongates the pulse, decreasing the peak intensity but increasing the pulse duration. In both cases, as we progress from

$N = 1$ to $N = 3$, and further to $N = 5$, there is a discernible increase in the ionization rate with the number of cycles. This trend is indicative of the cumulative effect of the electric field on the atom: more cycles mean more opportunities for the atom to absorb energy, leading to a higher probability of ionization. The data suggest that for a C atom, which has a relatively moderate ionization potential, the increased exposure to the laser field (as offered by more cycles) plays a more critical role in ionization than the peak intensity alone. Particularly for the higher chirp condition (Fig. 5(b)), it is important to state that despite the reduction in peak intensity, the ionization rate for $N = 5$ surpasses that of $N = 1$ and $N = 3$, reinforcing the idea that the duration of interaction is crucial in the ionization process. This extended interaction time allows for a progressive energy absorption by the atom, which is vital in reaching the ionization threshold, especially at intensities that do not drastically exceed it. These findings are consistent with the broader body of research [30-33] which posits that both the energy per unit time and the time over which the energy is delivered are pivotal to the ionization dynamics. Consequently, this analysis reaffirms the significance of chirp and number of cycles in controlling the ionization rates, presenting insights valuable for the optimization of laser parameters for specific ionization-driven applications.

4. CONCLUSION

In this paper, we have analyzed how chirped femtosecond laser pulses affect the ionization dynamics of atoms essential in biological and material sciences. Our results indicate that the chirp parameter significantly influences ionization rates, which is consistent with the notion that both the energy content of the pulse and its temporal distribution are decisive factors in ionization processes. We have shown that for pulses with higher chirp values, which correspond to stretched pulse durations, the ionization rates increase. This increase occurs despite a decrease in peak intensity, suggesting that a longer interaction time between the laser pulse and the atomic system is beneficial for the ionization process. This finding is important for applications where controlled ionization is critical, such as in precision surgery or material processing, where it is desirable to minimize damage to surrounding areas. Furthermore, our findings suggest that higher peak intensities associated with lower chirp values do not automatically translate into higher ionization rates. This can be particularly true for atoms with higher ionization potential, where the shorter pulse duration may not provide enough time for the atom to absorb the necessary energy to ionize.

The relationship between the number of cycles and ionization rates was also explored, revealing that increased cycles lead to higher ionization rates. This

observation is aligned with the current understanding that the cumulative effect of the electric field over multiple cycles can enhance the probability of ionization. Our study reaffirms the nuanced control that chirped laser pulses offer over ionization dynamics and underscores the importance of tailoring laser parameters to the specific needs of the application. While the theoretical framework provides a robust platform for predicting ionization dynamics, continued exploration of these phenomena remains crucial for the advancement of laser technology and its applications. In summary, by bridging the gap between theoretical predictions and experimental observations, this work contributes to the foundational knowledge in laser physics and opens up pathways for the development of new techniques in controlling and utilizing ionization dynamics for practical applications.

ACKNOWLEDGEMENTS. Authors would like to acknowledge the support received from the Science Fund of the Republic of Serbia, #GRANT 6821, Atoms and (bio)molecules-dynamics and collisional processes on short time scale -ATMOLCOL. Our appreciation also goes to the Serbian Ministry of Education, Science and Technological Development (Agreement No. 451-03-66/2024-03/ 200122).

LIST OF REFERENCES

1. M. Zamfirescu, M. Ulmeanu, F. Jipa, I. Anghel, S. Simion, R. Dabu, and I. Ionita, Rom. Rep. Phys. **62**(3) (2010) 594-609.
2. C.C. Shu, D. Dong, I.R. Petersen, and N.E. Henriksen, Phys. Rev. A **95**(3) (2017) 033809.
3. R. Dabu, Rom. Rep. Phys. **75** (2023) 405.
4. K. Amini, A. Chacón, S. Eckart, B. Fetić, and M. Kübel, Eur. Phys. J. D **75** (2021) 1-22.
5. V.M. Petrović, H.S.D. Marković, and I.D. Petrović, Results in Phys. **53** (2023) 107005.
6. H. Delibašić-Marković, V. Petrović, and I. Petrović, Rom. Rep. Phys. **76** (2024) 201.
7. R. Marani and E.J. Robinson, J. Phys. B: At. Mol. Opt. Phys. **32**(3) (1999) 711.
8. V. Stancalie, V. Pais, A. Mihailescu, O. Budriga, and A. Oprea, Rom. Rep. Phys. **62**(3) (2010) 528-545.
9. S. Li, B. Jochim, J. Stamm, D. Peng, H.C. Shao, J.M.N. Djiokap, and M. Dantus, Phys. Rev. A **105**(5) (2022) 053105.
10. W. Cho, J.U. Shin, and K.T. Kim, Sci. Rep. **11**(1) (2021) 13014.
11. M. Devi, H. Wang, S. Moon, S. Sharma, and V. Strauss, Adv. Mater. **35**(38) (2023) 2211054.
12. F. Zhu, X. Liu, Y. Guo, N. Wang, L. Jiao, and A. Liu, Chin. Phys. B **30**(9) (2021) 094209.
13. T. Ding, M. Rebholz, L. Aufleger, M. Hartmann, V. Stooß, A. Magunia, P. Birk, G.D. Borisova, D. Wachs, C. da Costa Castanheira, and P. Rupprecht, Nat. Commun. **12**(1) (2021) 643.
14. K. Varga-Umbrich, J.S. Bakos, G.P. Djotyan, P.N. Ignácz, B. Ráczkevi, Z. Sörlei, J. Szigeti, and M.Á. Kedves, Laser Phys. 26(5) (2016) 055006.
15. E. Neyra, F. Videla, J.A. Pérez-Hernández, M.F. Ciappina, L. Roso, and G.A. Torchia, Eur. Phys. J. D **70** (2016) 1-6.
16. Y.I. Salamin and S. Carbajo, Front. Phys. **7** (2019) 2.
17. V. Prasad, B. Dahiya, and K. Yamashita, Phys. Scripta **82**(5) (2010) 055302.
18. N. Teeny, E. Yakaboylu, H. Bauke, and C.H. Keitel, Phys. Rev. Lett. **116**(6) (2016) 063003.
19. T. Nakajima, Phys. Rev. A **75**(5) (2007) 053409.

20. Y. Cui, G.B. Zhang, Y.Y. Ma, D.B. Zou, X.H. Yang, M. Chen, J.X. Liu, Z.Y. Ge, L.C. Tian, L.F. Gan, and F.Q. Shao, Plasma Phys. Control. Fusion **61**(8) (2019) 085023.
21. T. Brabec and F. Krausz, Rev. Mod. Phys. **72**(2) (2000) 545.
22. T. Asavei, M. Tomut, M. Bobeica, S. Aogaki, M.O. Cernaianu, M. Ganciu, S. Kar, G. Manda, M. Mocanu, L. Neagu, and C. Postolache, Rom. Rep. Phys. **68**(Supplement) (2016) S275-S347.
23. S. Gales, D.L. Balabanski, F. Negoita, O. Tesileanu, C.A. Ur, D. Ursescu, and N.V. Zamfir, Phys. Scripta **91**(9) (2016) 093004.
24. S. Li, B. Jochim, J. Stamm, D. Peng, H.C. Shao, J.M. Ngoko Djiokap, and M. Dantus, Phys. Rev. A **105**(5) (2022) 053105.
25. M.C. Stroe, A.I. Florescu, M. Fifirig, F.W. Tamo, V. Ngassam, O. Motapon, and I.F. Schneider, Rom. Rep. Phys. **57**(4) (2005) 801.
26. J. Telles, Int. J. Numer. Methods Eng. **24**(5) (1987) 959-973.
27. E.M. Stein, Beijing Lect. Harmon. Anal. **112** (1986) 307-355.
28. K. Kuetemeyer, J. Baumgart, H. Lubatschowski, and A. Heisterkamp, Appl. Phys. B **97** (2009) 695-699.
29. F. Zhu, X. Liu, Y. Guo, N. Wang, L. Jiao, and A. Liu, Chin. Phys. B 30(9) (2021) 094209.
30. H. Ghaforyan, R. Sadighi-Bonabi, and E. Irani, Adv. High Energy Phys. **2016**(1) (2016) 2609160.
31. P.G. de Alaiza Martínez, A.C. La Fontaine, C. Köhler, and L. Bergé, J. Phys. B: At. Mol. Opt. Phys. **48**(9) (2015) 094010.
32. S.M. Young, H. Häffner, and M. Sarovar, Phys. Rev. Res. **5**(1) (2023) 013027.
33. S. Kumar Giri, U. Saalmann, and J.M. Rost, Phys. Rev. Lett. **124**(11) (2020) 113201.